ELSEVIER

Journal of Structural Geology 28 (2006) 1658–1669

JOURNAL OF STRUCTURAL GEOLOGY

www.elsevier.com/locate/jsg

Riedel-shear control on the development of pennant veins: Field example and analogue modelling

Sara Coelho [a,*], Cees Passchier [a], Fernando Marques [b]

[a] *Department of Earth Sciences, University of Mainz, Becherweg 21, 55099 Mainz, Germany*
[b] *Department of Geology and CGUL, University of Lisbon, Lisbon, Portugal*

Received 1 December 2005; received in revised form 17 May 2006; accepted 29 May 2006
Available online 26 July 2006

Abstract

The wall rocks of a crustal scale sinistral ductile shear zone in Namibia, the Purros Mylonite Zone, contain two types of asymmetric quartz veins. Bedding surfaces contain sigmoidal quartz veins with limited thickness along their symmetry axes that can be classified as tension gashes. A second type of veins consists of a striated central fault vein separating pennant-type quartz filled terminations. The tips of these ''pennant veins'' have a different orientation to those of the tension gashes. Analogue experiments were carried out using a sheet of silicone powder suspended on a slab of poly-dimethyl-siloxane (PDMS), both deformed in simple shear. These experiments produced open fractures very similar to the pennant veins that form by intersection of R and R' Riedel shear fractures. These fractures rotate and slip during progressive deformation, opening pennant shaped gaps. We interpret the natural pennant veins to form by the same mechanism of R and R' shear fracture initiation, and subsequent rotation and opening. Since this mechanism differs from that of previously described vein types such as wing cracks, tension gashes and swordtail or fishmouth termination veins, which mainly open as tension veins, we consider pennant veins as in new independent class of asymmetric mineral-filled veins.

1. Introduction

Veins are extension fractures filled with mineral deposits, commonly quartz or calcite, and one of the most common features in deformed rocks of all types and metamorphic grades. Opening of veins is structurally controlled by orientation of fractures in a volume of rock but other parameters, like pore fluid pressure or porosity, are also important. Single or *en échelon* tension gashes (Fig. 1a; e.g. Ramsay and Huber, 1983; Olson and Pollard, 1991), wing cracks (e.g. Horii and Nemat-Nasser, 1985; Willemse and Pollard, 1998) and swordtail terminations in boudin parting surfaces (Swanson, 1992) are common examples of veins developed as mode I extension fractures. As such, they can be used in the interpretation of bulk flow kinematics and are an important source of information on the deformation history of the host-rock, especially if associated with fibres (e.g. Bons, 2000; Köhn et al., 2000; Hilgers and Urai, 2002). However, pure tension fractures are not the only structural control on the development of veins. This paper explores an alternative way of opening space for mineral deposition controlled by Riedel (R) and anti-Riedel (R') conjugate shear fractures.

Riedel shear fractures were first recognised as a principal feature of brittle to semi-brittle shear zones by Riedel (1929), who produced these structures in analogue experiments with clay. The subject has since been the focus of extensive research in field studies (e.g. Moore, 1979; Davis et al., 1999; Ahlgren, 2001; Katz et al., 2004), analogue modelling with clay (e.g. Cloos, 1955; Wilcox et al., 1973; Tchalenko, 1968; Smith and Durney, 1992; Marques, 2001) and sand (e.g. Naylor et al., 1986), direct shear experiments (e.g. Bartlett et al., 1981; Moore and Byerlee, 1992; Schreus, 1994) and numerical modelling (e.g. Dresen, 1991; Braun, 1994; McKinnon and Garrido de la Barra, 1998). These works resulted in a widely accepted model of shear fracture orientation in non-coaxial deformation, illustrated in Fig. 1b. The most

* Corresponding author.
E-mail address: sarasscoelho@yahoo.co.uk (S. Coelho).

0191-8141/$ - see front matter © 2006 Elsevier Ltd. All rights reserved.
doi:10.1016/j.jsg.2006.05.009

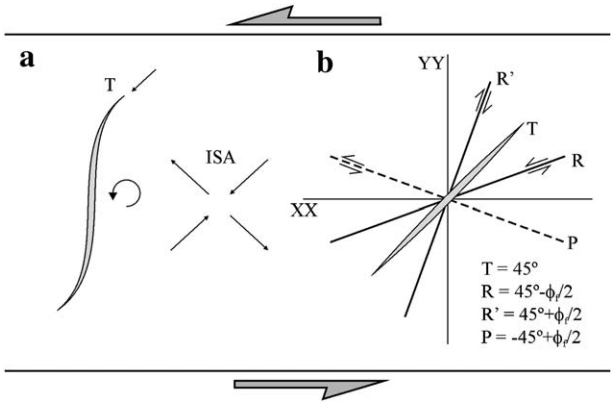

Fig. 1. (a) Geometry of an idealised tension gash in sinistral simple shear. ISA, instantaneous stretching axes; (b) theoretical distribution of tensional fractures (T) and shear fractures (R, R' and P) in the same kinematical framework. ff, internal friction angle.

conspicuous element of this idealised geometry is the Riedel conjugate set, comprising synthetic Riedel fractures (R) and conjugate antithetical Riedel fractures (R'), oriented at $45^\circ \pm \phi/2$, where ϕ is the internal angle of friction of the rock. Also important are synthetical P-shear fractures (at $-45^\circ + \phi/2$) and the purely tensional T fractures (at 45° in simple shear). The precise angular relationships of the different sets of fractures and the shear plane are dependent on the internal angle of friction, as well as on the strain rate and stress state (Ahlgren, 2001) and vorticity (Smith and Durney, 1992). This framework is generally interpreted as a precursor to faults in a synthetically driven model (e.g. Ahlgren, 2001) where R fractures are the first to develop, followed by P fractures. This paper investigates the influence of $R-R'$ conjugate fractures as structural controls on veins, following the work of Swanson (1992), who suggested that R fractures had some role in the kinematics of vein terminations. This paper also introduces *pennant veins*, a new type of vein geometry, based on field observations in Namibia and analogue modelling.

2. Geological setting

The Kaoko Belt in Namibia is a NNW trending, oblique convergent orogen, divided into three zones (Goscombe et al., 2003a, 2005a,b; Konopásek et al., 2005; Fig. 2). The *West Kaoko Zone* (WKZ) includes basement composed of Panafrican migmatites and granites with amphibolite to granulite metamorphic facies (Goscombe et al., 2003b, 2005a). The *Central Kaoko Zone* (CKZ) comprises a Paleoproterozoic basement of migmatitic and gneissic rocks with a Neoproterozoic cover of deep basin and slope facies (Damara sequence; Goscombe et al., 2003a; Konopásek et al., 2005). Metamorphic conditions on the CKZ grade from upper-amphibolite facies in the West to lower greenschist facies in the East

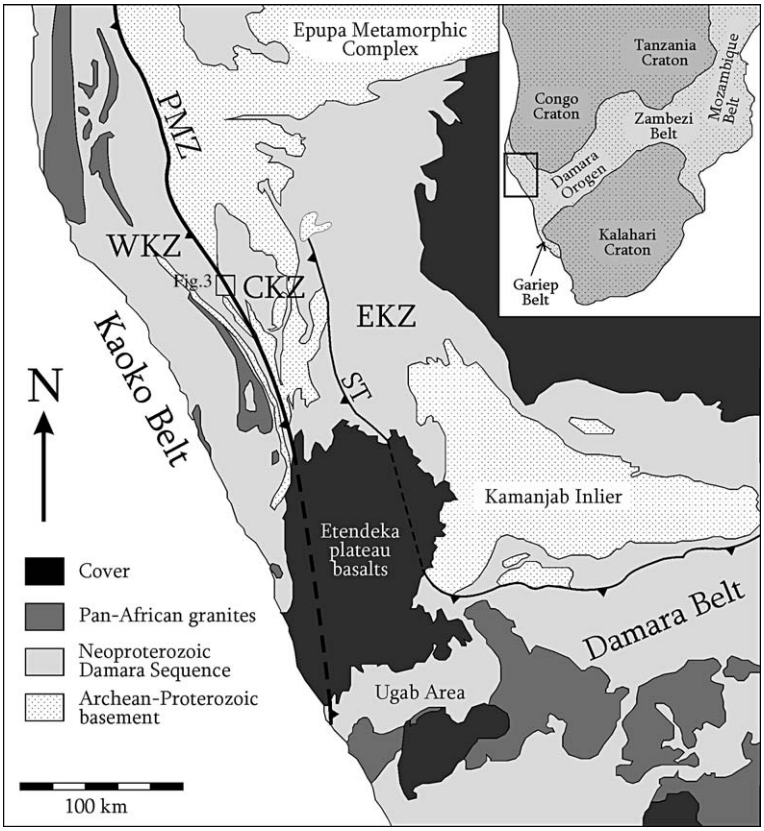

Fig. 2. Regional geology of the Kaoko Belt; studied area shown by a square. Inset: location of the Kaoko Belt with respect to the major cratons and mobile belts in Southern Africa. WKZ, CKZ and EKZ: Western, Central and Eastern Kaoko Zones. ST, Sesfontein thrust. PMZ, Purros Mylonite Zone. Simplified from Goscombe et al. (2003a, Fig. 1).

(Goscombe et al., 2003b, 2005a; Konopásek et al., 2005). The *East Kaoko Zone* (EKZ) represents the foreland of the orogen and comprises subgreenschist Damara sequence rocks of shelf facies (Goscombe et al., 2003a,b). The WKZ and CKZ are separated by the Purros Mylonite Zone (PMZ), a crustal-scale, sub-vertical and sinistral strike-slip ductile shear zone, with a length of over 400 km extending from the South of Angola to the Ogden Rocks in the East of the Ugab zone (Passchier et al., 2002).

Deformation in the Kaoko Belt consists of three tectonic phases, the first of which (M1) only occurs in the WKZ (Goscombe et al., 2003a, 2005b; Konopásek et al., 2005). The second deformation phase (M2), active between 580 and 550 Ma, was dominated by transpressive deformation at peak metamorphic conditions and during cooling, progressing from a wrench stage (M2w) to a convergent stage (M2c) (Goscombe et al., 2003a). The wrench stage is related to activity of the PMZ and resulted in pervasive and intense non-coaxial deformation that produced the dominant LS-fabric in the area. The convergent stage is considered continuous with the wrench stage and develops pervasive east-vergent folds with shallow plunging axes. These folds do not develop axial planar cleavage, although crenulation cleavage parallel to early M2w lineations is common in selected rock types. The axial plane varies in dip across the orogen and defines a large scale asymmetric flower structure, centred on the PMZ and evolving to the East as west dipping, progressively shallower, east-vergent nappes (Goscombe et al., 2003a). The third deformation phase (M3, between 535 and 505 Ma) resulted in North–South shortening of the orogen and produced large scale upright folds without an axial planar foliation. With these features, the Kaoko Belt represents a Neoproterozoic, crustal scale, sinistral transpressional orogen with flower structure architecture (Goscombe et al., 2003a, 2005b).

This study focuses on an area located near Orupembe which straddles the border between the WKZ and CKZ zones including outcrops of the Purros Mylonite Zone (Fig. 3). In Orupembe, the WKZ consists of a Neoproterozoic low grade turbiditic sequence with M2 deformation features. The PMZ is about 2 km wide, steeply dipping (60–70°) to the West and includes slivers of basement granitoid rocks. The CKZ locally consists of Paleoproterozoic basement comprising a granodioritic migmatite with hornblende and epidote layers overlain by pink orthogneiss with feldspar augen. The basement is covered by Mesoproterozoic quartzites and the Neoproterozoic Damara Sequence comprising (bottom to top) interbedded impure quartzites, calcsilicate rocks and micaschists, followed by diamictites and cap carbonates (Hoffman et al., 1994). The main deformation feature throughout the area is an LS fabric produced by the M2 wrench stage. The folation is generally gently dipping and parallel to bedding. It consist of recrystallised feldspar and epidote in the quartzitic and calcsilicate rocks, and aligned micas in the micaschist units. The lineation trends approximately NS and is a shallow plunging quartz-feldspar aggregate lineation (Fig. 4a). Associated shear sense criteria, such as mantled objects and rare shear bands, indicate sinistral shear sense consistent with the overall kinematics of the Purros Mylonite Zone. The foliation is steeply dipping near the PMZ and evolves to the East into open folds with a gently SSE plunging axis and sub-vertical axial plane (Fig. 4b). This folding is related to the M2 convergent stage and does not develop a regional axial planar cleavage. However, micaschist units present a NNW/SSE trending crenulation lineation parallel to the fold axis of the large scale folds. The quartzitic more competent units do not develop mesoscopic folding. Instead they present a new type of vein geometry, which is the main focus of this paper.

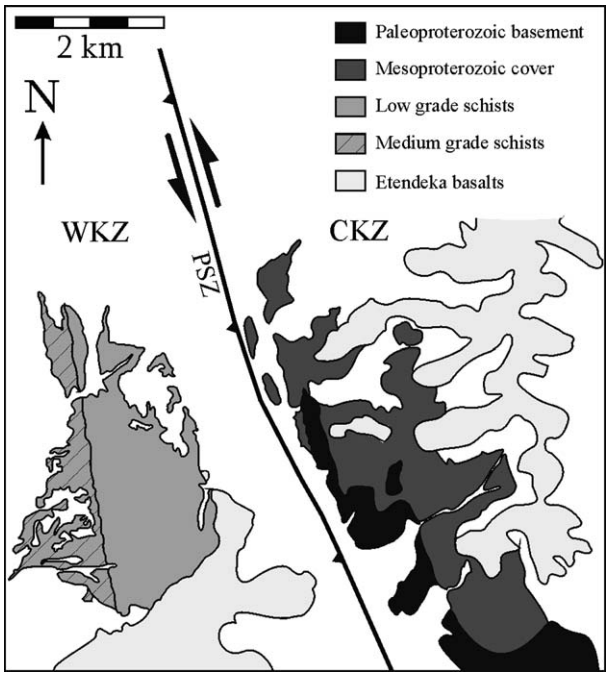

Fig. 3. Regional geology of the Orupembe area. W and CKZ, West and Central Kaoko Zone.

3. Quartz veins from the CKZ in Orupembe

Detailed field work in Orupembe revealed the presence of two different types of quartz veins (Figs. 5 and 6). Although the geometry of these veins is clearly distinct, they share common characteristics. Both occur in the same outcrops of quartzite interbedded with calcsilicate and micaschists layers and both represent sets of quartz veins developed under a metamorphic grade lower than that of the main stretching lineation, as suggested by their filling of quartz, less deformed than the host-rock, and the geometric cross-cutting of the main LS fabric. They are therefore late with respect to the main deformation that is ascribable to the wrench stage of the first deformation phase of the Kaoko Belt.

The first set of studied quartz veins has a typical sigmoidal geometry (Figs. 5 and 6a,b). They are up to 20 cm in total length and up to 1 cm wide. These veins are unusual since their sigmoidal shape is visible only on the foliation plane and cannot be easily observed in planes orthogonal to the S-fabric, where they are short and straight. The main aggregate lineation is locally deflected near the centre of the sigmoidal

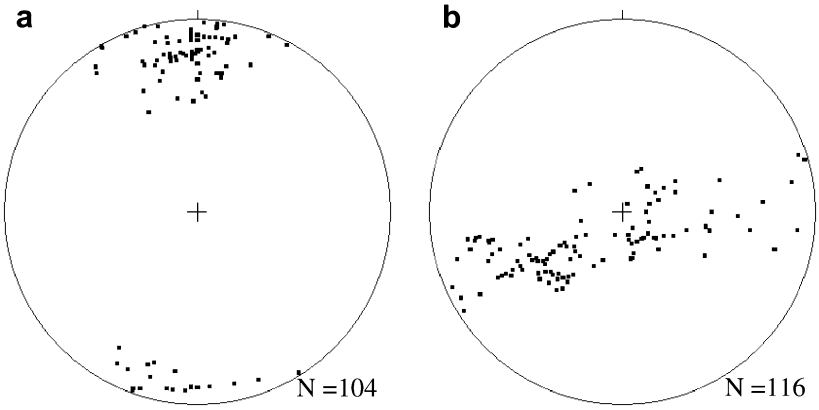

Fig. 4. Stereoplots representing field data for (a) stretching lineations and (b) foliations of the Orupembe area. *N*, number of measurements.

veins. The tips and centres of these sigmoidal veins were measured as lines within the foliation plane, as summarised in Table 1. Tips define an average 77° angle with the lineation, whilst the centres are relatively less inclined with an average angle of 34°. In some examples, a younger vein generation cuts the central part of the veins with the same orientation as the tips (Fig. 6a). The veins are interpreted as sigmoidal tension gashes, developed by progressive deformation of a quartz-filled tensional fracture oriented according to the maximum shortening instantaneous stretching axis (ISA) (cf. Fig. 1a; Ramsay and Huber, 1983; Passchier and Trouw, 2005).

The second type of quartz veins has been observed in shallow dipping quartzitic units and has different characteristics (Figs. 5 and Fig. 6c,d). These veins cut both the foliation and the aggregate lineation and can be observed in all surfaces of the outcrop. In the foliation plane, they present distinct triangular pennant-shaped terminations, hence the name *pennant veins*. These structures are up to 10 cm in length, measured in the foliation plane. The interconnecting surface (IS) is 5–20 cm wide and is usually not mineralised, although in some cases quartz is present uniting the pennant terminations in a single quartz vein. The orientation of the external surface (ES) of the pennants and interconnecting surface (IS) was measured in the field with results presented in Fig. 7 and Table 1. The ES is approximately orthogonal to the regional NS lineation; the IS is less inclined to this fabric, with an average 20° angle to the external surface. The IS planes contain elongate white mica grains and striae, with shallow plunge to the SW and criteria suggesting downward motion of the southern block (Fig. 5). The striae make a small angle with the intersection line of the foliation and the IS. The mechanism causing the development of the pennant veins and associated features was not clear from field observations alone and we therefore decided to use analogue modelling as described below.

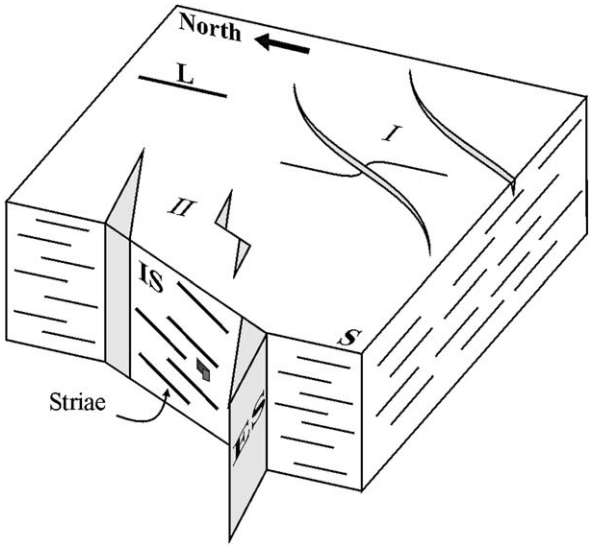

Fig. 5. Schematic drawing of sigmoidal (I) and pennant veins (II) as they occur in outcrop. Orientations are exaggerated with respect to the averages shown in Table 1. IS and ES are interconnecting and external surface. Not to scale.

4. Analogue modelling

Analogue experiments were carried out in a deformation rig described in Marques and Coelho (2001) and used subsequently in several other studies (e.g. Bose and Marques, 2004; Marques and Bose, 2004). This machine produces parallel-sided plane strain sinistral simple shear deformation imposed on the model by dislocation of one of the side walls. The far-field strain rate set by the machine was constant throughout the runs at 10^{-3} s^{-1}.

The experimental set up design (Fig. 8) was based on field observations and attempts to reproduce the geological setting of the veins as described above. It was assumed that the veins developed in non-coaxial flow, with vertical shear planes imposed on a horizontal or gently dipping foliation plane. The alternating micaschist/quartzite metasedimentary sequence is represented by two layers of different materials, transparent PDMS and white silica powder. Poly-dimethyl-siloxane (PDMS; manufactured by Dow Corning of Great Britain under the trade name of SGM 36) is a polymer with Newtonian properties at room temperature, which has been extensively used in experimental modelling as analogue of viscous materials (see Weijermars, 1986 for properties). This material was used to simulate the micaschist layers, where fractures have

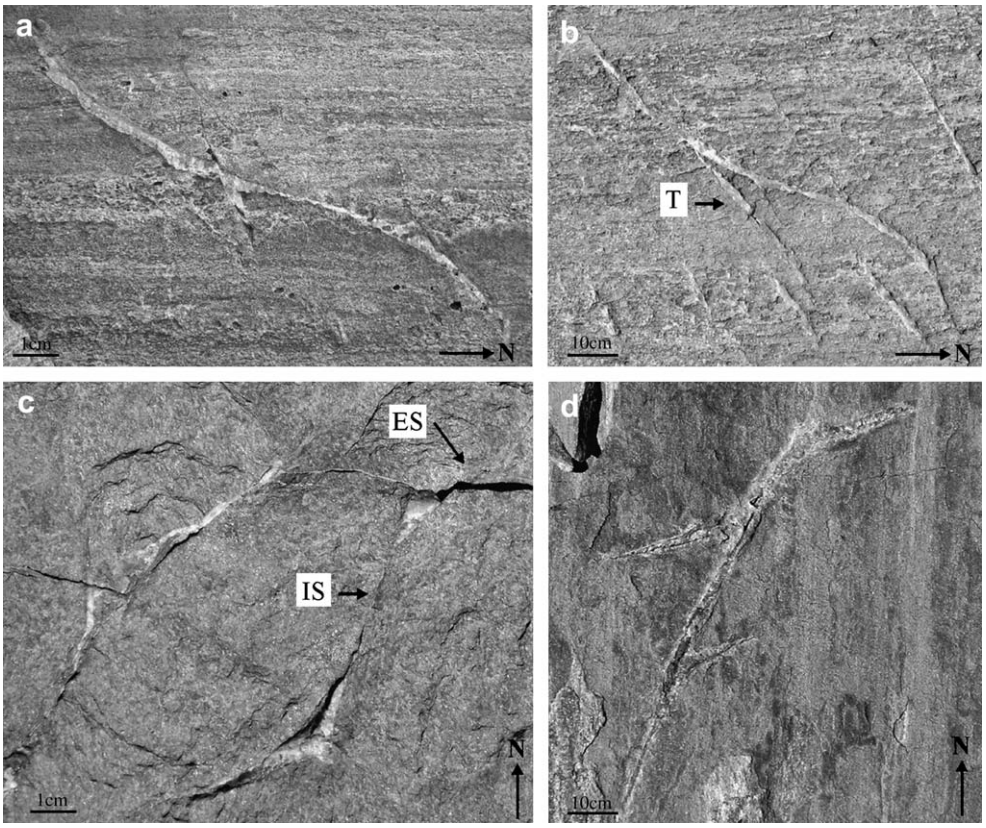

Fig. 6. Field examples of sigmoidal tension gashes (a,b) and pennant termination veins (c,d). *T*, tensional fracture (cf. Fig. 1); IS and ES, interconnecting and external surfaces. All photos parallel to foliation plane.

not been observed, and was in complete adherence with the rig's side walls. On top of the PDMS (Fig. 8), a layer of fine-grained (20 μm) silica powder was placed to represent the quartzite units. This material has cohesion of 300 Pa and fails according to a Coulomb criterion (Krantz, 1991). Similar powdered silica has been used as an analogue for the brittle upper crust in experiments by Galland et al. (2003). The silica powder layer was built by sieving with the help of a sugar sprinkler cooking device, from a height of about 10 cm. By using the same handling technique, physical properties of the silica powder such as density, cohesion and internal angle of friction are assured to remain similar in all runs (Krantz, 1991). The observation surface was imprinted with a grid of markers in five of the experimental runs. These markers provided a gauge for dislocation (or slip) in the developing R/R' systems.

Table 1
Summary of field measurements on the two sets of veins

	Tips			Centres		
Sigmoidal veins (lines to L)	Av	σ	*N*	Av	σ	*N*
	77	20.2	96	34	16.5	52
Pennant veins (poles to planes)	Av ES	*N*	Av IS	*N*	Av Str	*N*
	175/90	34	161/85	82	247/17	54

Av, average; ES/IS, external/internal surface; Str, striae; N, number of measurements.

The boundary conditions imposed by the setup of the experiments specify that deformation is transmitted, point by point, to the silica powder from the PDMS underneath, not by push from the confining walls. The silica powder is unconfined in the vertical direction. The setup further determines that the simple shear plane is orthogonal to bedding, which is in good agreement with the fact that the field examples occur on the foliation plane.

The evolution of fracture orientation with progressive deformation is described by the angle ϕ, measured between the fracture and the *X*-axis of finite strain (Fig. 8). Counter clockwise angles were considered positive; this corresponds to synthetic rotation of the fractures in the given sinistral shear sense. For every run the orientation of fracture sets was measured at shear strain gamma values of 0.125, 0.25, 0.5, 0.75 and 1.0γ. Although the rig is capable of attaining higher shear strains (up to 12γ), the experiments were limited to a maximum of 1.25γ. After this amount of shear strain, the observation surface was disrupted in such a way that it was virtually impossible to follow the evolution of individual sets of fractures any further. This is also the reason why the number of measurements in the latest stages of the experiments is less than for the initial part (Table 2): in numerous examples, the individual shear fractures were lost in the disrupted surface after a certain amount of deformation.

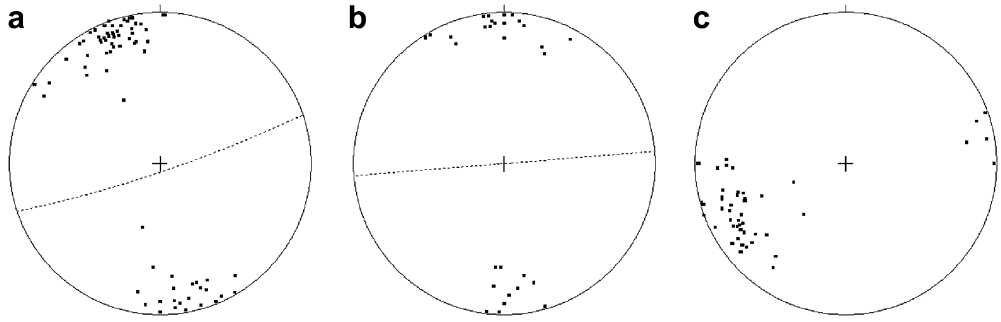

Fig. 7. Field measurements of flag veins, summarised in Table 1. (a) interconnecting surface; (b) external surface and (c) striae.

5. Experimental results

The results of 20 experimental runs are summarised in Table 2 and presented in graphical form in Fig. 9a. All angles were measured with respect to the shear zone boundary, represented in the analogue experiments by the shear rig wall.

The first noticeable effect of deformation in the silica powder was, in all runs, the development of $R-R'$ shear fractures, either isolated or organised in conjugate sets, such as in Fig. 10i. Riedel shear fractures (R) appeared with an average orientation of 21°, whilst conjugate-Riedel shear fractures (R') were as expected more steeply oriented, at ca. 73° (Table 2, Fig. 9a). The first measurement was made in all instances at 0.125γ, and it is therefore highly probable that these orientations have already a certain amount of rotation with respect to the original angle of the shear fracture at instantaneous deformation. Once established, the R- and R'-shear fractures follow different paths. R'-shear fractures experience consistent synthetical rotation, albeit about 5° less than expected for a material line with corresponding initial orientation (Fig. 9a). This is in agreement with the observation that shear strain is underestimated if calculated by the rotation of R'-shear structures, since other mechanisms, such as slip and rigid block rotation, may be present to accommodate deformation (Katz et al., 2004). R-shear fractures have a more variable behaviour and may or may not rotate continuously as their conjugate structures. Fig. 9b represents an example run (#13) and although at first examination the rotation of the group might seem uniform, focussing on individual R-shear fractures shows intrinsic differences. Fracture I (Fig. 9b), for example, rotates synthetically, just as the R' counterparts, but fracture II, and several others, undergo limited rotation remaining within ±5° of their initial orientation, with possible back rotation in some examples. A similar behaviour of R-shear fractures was reported by Swanson (1992) in analogue modelling with clay. This dual behaviour was observed in all runs and accounts for the increasing standard deviation values of R-shear fractures with progressive deformation (Table 1, Fig. 9a).

Markers imprinted on the observation surface show that slip occurred in both R and R' and that these structures are mode II fractures (Fig. 11). The observed displacement is consistent with that expected for R-R' systems and can be an important criterion to distinguish modelled structures from previously described features (Section 6.1). The amount of slip (displacement parallel to the fracture orientation) was measured, subsequently normalised considering the side of the grid as unit and plotted against rotation angles (Fig. 11a). Experimental results show that slip is inversely related to the amount of rotation: fractures that rotate more experience less slip. Conversely, fractures that rotated less, remained stable or back-rotated show more slip. In these cases, deformation was accommodated not by rigid rotation but mostly by displacement parallel

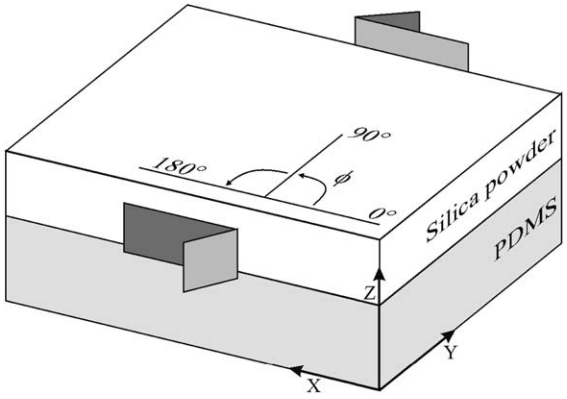

Fig. 8. Experimental setup. X, Y and Z are the kinematic axis. PDMS and silica powder were the analogue materials. Shear sense was sinistral in all runs. Shear fracture orientation was measured from the X-axis (f) and considered positive when counter-clockwise. Not to scale.

Table 2
Summary of the experimental results, shown by average and standard deviation

Type	γ	Average	σ	Max	Min	N
R	0.125	21.69	5.63	36	10	57
	0.25	24.13	7.05	46	10	109
	0.5	28.70	8.06	59	8	128
	0.75	34.02	10.85	69	14	119
	1	37.58	13.66	66	12	74
	1.25	37.00	12.79	71	22	29
R′	0.125	73.45	6.83	87	54	122
	0.25	78.84	7.38	99	57	136
	0.5	91.13	9.64	111	65	144
	0.75	105.08	10.61	126	77	127
	1	114.90	9.66	138	96	79
	1.25	119.86	7.95	138	105	39

N, number of measurements; Max and Min, the maximum and minimum values observed.

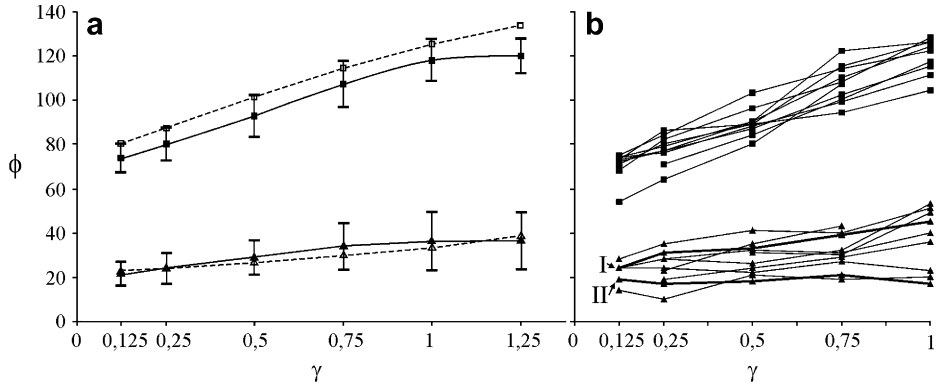

Fig. 9. Evolution of shear fracture orientation as obtained in the experimental results. Closed squares and triangles represent experimental R'- and R-shears, respectively. (a) average of 20 runs with standard deviation represented as error bars; open squares and triangles represent the orientation expected considering the rotation of a material line. (b) Orientations measured in example run (#13). Bold lines I and II are individual fractures. See text for discussion.

to the fracture orientation. Fig. 11a also shows that R and R' fractures that rotated continuously (I) show a smaller amount of slip compared to the R fractures which remained stationary or back rotated (II).

With progressive deformation, the slip systems operating in the obtuse angle between conjugate R–R' shear fractures induce slipping in opposed sense that develops into gaps with pennant shapes (Fig. 10), combined with shear fracture rotation. Converging slip sense explains why no gaps were observed in the acute angle between the shear conjugates. The opening is further enhanced by the orientation of the shear fractures with respect to the ISA. Since the experiments were performed under simple shear conditions, the ISA are known to be at angles of 45° (maximum shortening) and 135° (maximum stretching) with the *flow plane* (Fig. 10), thus favouring opening of the shear fractures in the first steps of deformation. When the fractures rotate enough, such as the R' that reach higher ϕ-values, they enter the shortening field and, instead of opening they become prone to shortening normal to the vein surface (Fig. 10iv,v). The pennant gaps however persisted in all runs, even when the R'-shear fracture was in the shortening field. R' fractures oriented in this field

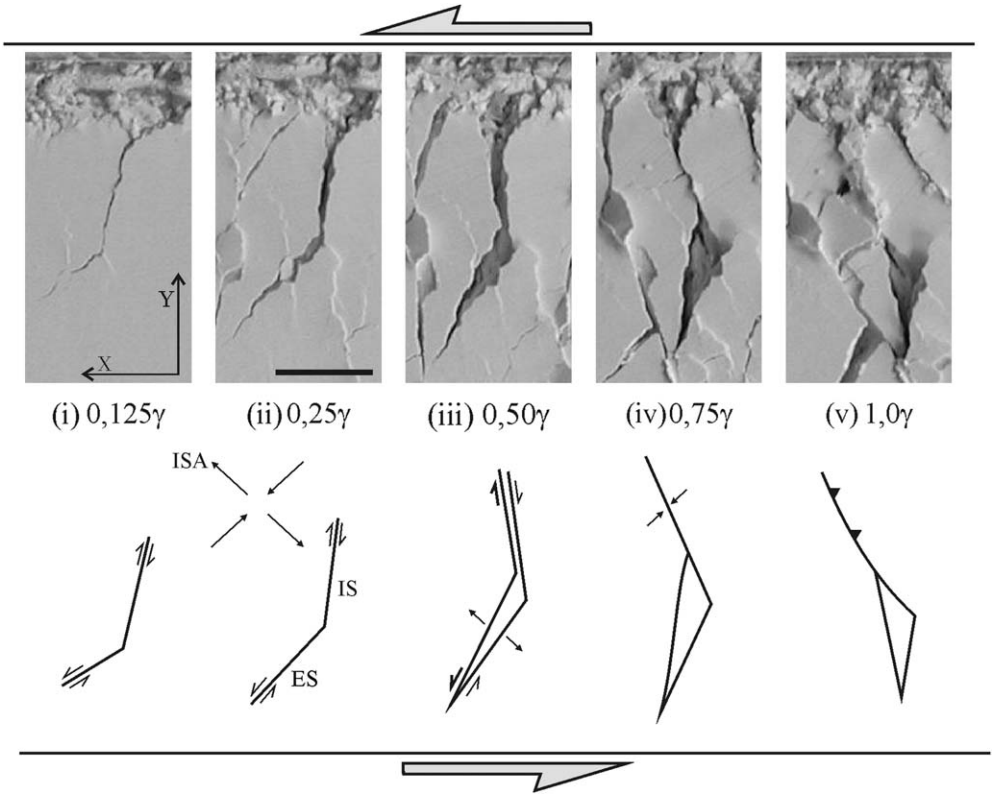

Fig. 10. Development of triangular gaps controlled by R and R' shear fractures. Experimental example from run #3 at 0.125/0.25/0.5/0.75 and 1 γ (i–v) and corresponding sketches. ES and IS as in previous figures. Scale bar represents 1 cm valid for all photos.

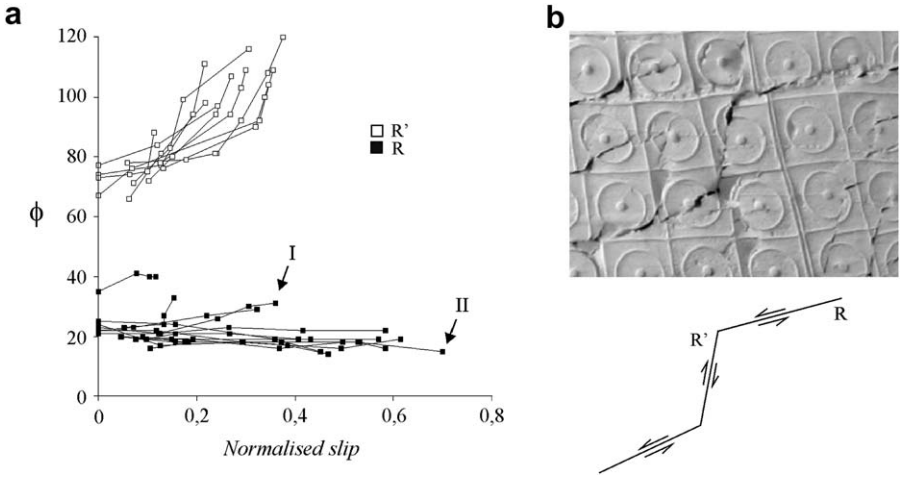

Fig. 11. (a) Comparison between amount of rotation (f) and slip. Note that lines parallel to the *xx*-axis represent pure slip with no rotation and lines parallel to the *yy*-axis represent pure rotation with no slip. Note also that the larger amounts of slip correspond to the smaller amounts of rotation. I highlights a fracture that rotated continuously; II highlights a fracture that back-rotated. (b) Thumbnail of run #17 for 0.25 γ, with operating slip systems in $R-R'$ fractures. Grid side is 1 cm. See text for discussion.

often display minor thrusting of the right block over the left (Fig. 10v). The example of Fig. 10, although illustrative of the problem, represents the special case where both *R*- and R'-shear fractures rotate continuously. The majority of pennant gaps in the experiments however occur in the cases where the R'-shear rotates continuously whilst the *R*-shear tends to remain stable (Fig. 12a).

R'-shear fractures are usually considered to be relatively late and confined to the overlap areas of the dominant *R* fractures in the general theoretical model of shear fractures (e.g. Ahlgren, 2001). However, in the present series of experiments, R' fractures clearly dominated over *R*, suggesting that the subordinate role of R' is not a universal rule. Similar behaviour has been reported in previous studies based on field examples (e.g. Ahlgren, 2001; Katz et al., 2004).

6. Interpretation and discussion

The gaps observed in the experimental runs (Figs. 10 and 12) and described in the previous section are interpreted here as the space available in Nature for the deposition of the pennant-shaped quartz veins observed in the field (Fig. 6c,d). As their analogue equivalents suggest, the geometry and orientation of the termination features, filled in Nature by quartz, are also controlled by the kinematics of $R-R'$ shear fractures operating in the quartzite units.

6.1. Comparison of pennant veins with previously described structures

Wing cracks (Horii and Nemat-Nasser, 1985; Willemse and Pollard, 1998), splay fractures (Martel and Pollard, 1989; Cooke, 1997) or crack kinks (Nemat-Nasser and Horii, 1982; Cruikshank et al., 1991) are tension fractures associated with non-propagating fault or shear fracture terminations (Fig. 13). They are mode I features, but occur as a result of slipping on a parent mode II fracture. Wing cracks do not develop in the central region of a fault, where energy is accommodated best by propagation of slip patches (Martel and Pollard, 1989). They are usually at a high angle to the parent fracture, dependent on the ratio between shear and normal stress, and variable between 0° (pure mode I) and about 70° (pure mode II) (Fig. 13b; Willemse and Pollard, 1998). Wing cracks are also commonly associated with solution

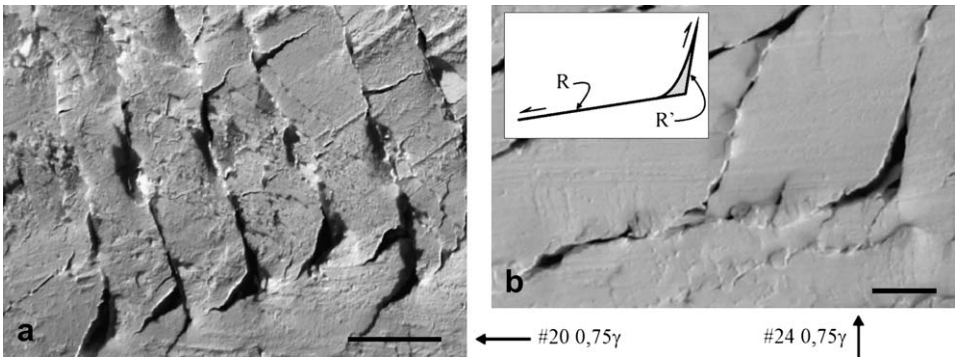

Fig. 12. Examples of triangular gaps: (a) controlled by R'-shears (cf. Fig. 10b) and (b) *R*-shear dominated (less common). Scale bars are 1 cm in length.

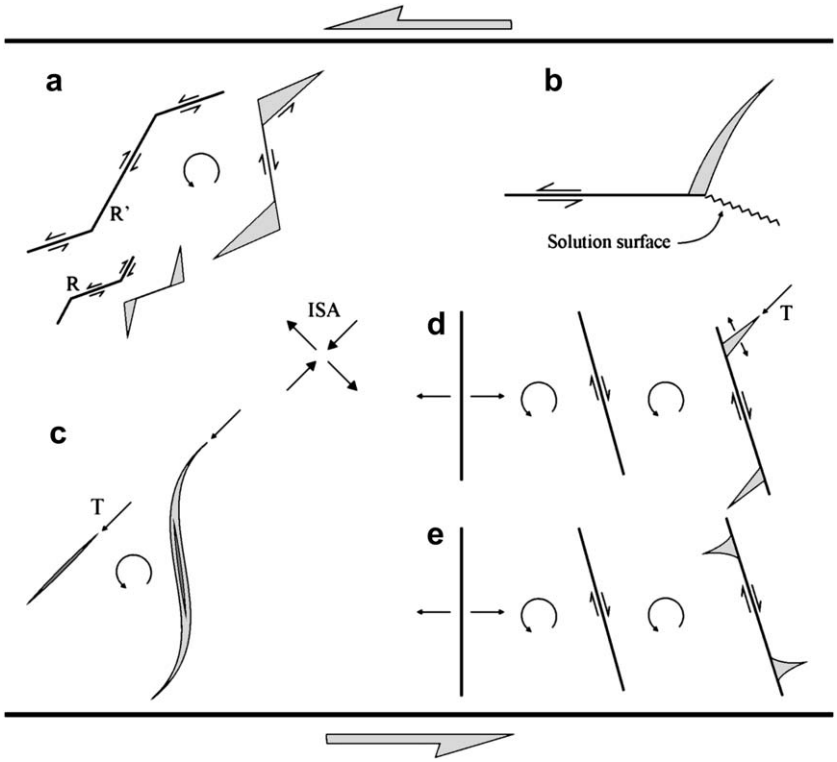

Fig. 13. Development of pennant veins compared to other structures. (a) Pennant veins: R'-controlled (more common) and R-controlled (less common); (b) wing cracks; (c) tension gashes; (d) swordtail terminations and (e) fishmouth terminations.

surfaces oriented orthogonal to the cracks (Fig. 13b; Willemse and Pollard, 1998). With progressive deformation, wing cracks tend to acquire a curved horn shape, pointing towards the maximum shortening axis (Horii and Nemat-Nasser, 1985; Nemat-Nasser and Horii, 1982). From a geometric perspective, wing cracks are similar to pennant veins, especially the ones controlled by R fractures (Fig. 12b). There are, however, important distinctions which make it necessary to define pennant veins as a separate category: (1) wing cracks are extensional mode I features, without slip on their surface, whereas pennant veins develop by combined rotation of and displacement in $R-R'$ mode II fractures (Fig. 11b). (2) The observed pennant veins are never associated with orthogonal solution surfaces or similar compression structures as wing cracks commonly are. If this was the case, the analogue examples would show perturbations on the surface at about 90° of the pennant termination, which are not present. (3) Wing crack orientation depends on the ratio between normal and shear stress, while pennant veins are controlled by $R-R'$ conjugate fractures. (4) Pennant veins observed in the field and analogue experiments preserve their typical straight shape, unlike wing cracks that tend to develop arcuate geometries pointing towards the maximum shortening of the ISA.

Tension gashes (e.g. Ramsay and Huber, 1983; Olson and Pollard, 1991) are tension fractures opened parallel to the maximum instantaneous stretching direction (Fig. 13c). With progressive deformation, this fracture may be filled as a vein and undergo synthetic rotation with respect to the overall shear sense (Fig. 13c). Combined continuous growth results in a typical sigmoidal geometry that can be used as a shear sense indicator (e.g. Ramsay and Huber, 1983; Passchier and Trouw, 2005). Tension gashes may be distinguished from pennant veins as follows: (1) they are structurally controlled by tension fractures T instead of Riedel conjugate fractures; (2) they are mode I fractures without displacement parallel to the vein direction, whereas in pennant veins slip is present (Fig. 11b) and plays a major role in development of the veins (Fig. 10); 3) in the first increment of deformation tension gashes appear at an angle of ca. 45° with respect to a simple shear zone wall, while pennant external surfaces are either considerably steeper (if controlled by R') or shallower (if controlled by R); (4) most tension gashes have a smooth, sigmoidal geometry, whereas pennant veins always have angular features.

Type I boudin parting surfaces (Hanmer, 1986) are pull-aparts developed normal to layering. With progressive deformation these surfaces rotate synthetically, producing antithetic slip with respect to the overall shear sense. According to Swanson (1992), these structures are privileged sites for the development of two types of asymmetric geometries, swordtail and fishmouth quartz-filled terminations (Fig. 14 in Swanson, 1992) which resemble pennant veins to some extent. Swordtail terminations are planar to arcuate fractures, developed in the extensional side of the boudin parting surface. In progressive deformation, the boudin parting surfaces rotate and oblique gash veins develop in their extensional side. Space available for quartz deposition in these oblique gashes is created by the slipping system operating in the boudin parting surface (Fig. 13d; Swanson, 1992). Fishmouth terminations result from the

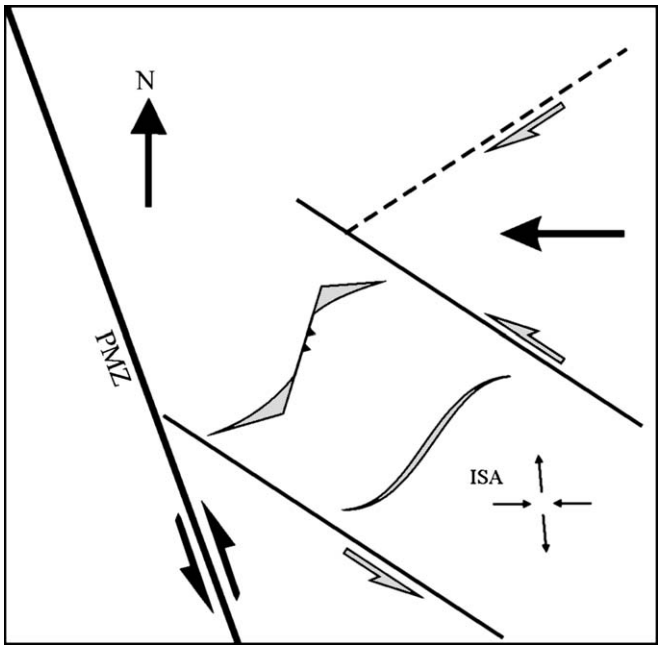

Fig. 14. Schematic representation of the studied veins in their geological context. PMZ and ISA as in previous figures. See text for discussion.

collapse of the contractional side of a boudin parting surface along a fault plane and disappear with further increments of deformation (Fig. 13e; Swanson, 1992); they can be easily distinguished from pennant veins by their contractional nature. Pennant veins are geometrically very similar to swordtail terminations and develop by the influence of slip on a pre-existing fracture. The difference resides in the type of fractures involved: swordtail terminations develop around tensional fractures (boudin parting surfaces and oblique gashes), whereas pennant veins are mode II fractures, opened by combined rotation and slip of $R-R'$ conjugates.

6.2. Kinematic interpretation of pennant veins

Gash-related features such as sigmoidal tension gashes, like the ones identified in the study area, or the swordtail terminations of Swanson (1992), are initially tensional fractures, parallel to the maximum shortening axis of the instantaneous stretching axes. In outcrop, these structures may present a distinctive sigmoidal shape where tips can be interpreted as gauges for the maximum shortening axis orientation (e.g. Ramsay and Huber, 1983). This observation allows sigmoidal tension gashes to be accurate shear sense indicators. The use of pennant veins as shear sense indicators is limited by their own characteristics. Since they develop on the extensional side of the shear fracture terminations, a statistical study of pennant vein orientation in outcrop can be used to estimate the location of the extension field of deformation. This, combined with other criteria such as boudin trails or folds, may be of use to determine shear sense. However, it is important to stress again that they are not parallel to the maximum shortening axis of the ISA, as the tips of tension gashes are, and therefore cannot be interpreted as indicators of this bulk flow element. The external surface of the pennant termination vein (Fig. 10) is controlled by the R-shear fracture, or less commonly by R' (Fig. 12), and shows the orientation of these features in a given stage of deformation. This information is difficult to use in kinematic interpretation because both R- and R'-shear fractures are expected to undergo rotation throughout progressive deformation and the specific amount of shear strain is usually unknown in natural examples. Moreover, the initial orientation of R- and R'-shear fractures is highly dependent on the rheological properties of the rock, namely the internal angle of friction and pore fluid pressure.

6.3. Contribution to regional geology

The style of development of the observed sets of sigmoidal tension gashes and pennant veins (Fig. 5) are the only field evidence that deformation in the Orupembe area continued into a stage of brittle deformation after the development of the mylonitic lineations and foliations. This deformation is late or at least coeval with the latest stages of the M2 wrench stage that produced the main fabric due to: (1) the fact that the sigmoidal veins cut and deflect the main lineation and (2) the metamorphic grade of the quartz veins that, according to their brittle nature, is lower than the upper greenschist/amphibolite facies of the main lineation (Goscombe et al., 2003b). What are the characteristics of the deformation that produced the veins?

As an answer to this question, pennant veins are not very informative because, as seen in the analogue modelling, the amount of rotation of the R/R' shear fractures is high even in the first steps of deformation. Moreover, in field example the initial orientation of the R/R' shear fractures is unknown and, since the veins occur on the foliation plane, the direction of the shear plane is also undefined. Sigmoidal veins also occur on the foliation plane, but they give important information about flow kinematics since the known tip orientation of these veins indicates the maximum shortening ISA, which is, in simple shear, related to the shear plane by an angle of 45°. Their field orientation suggests the existence of a WNW-ESE trending sinistral ductile simple shear zone, or general transpression with ISA at 70° to the PSZ affecting the entire Orupembe area and overprinting the previous stike-slip pattern (Fig. 14). This solution is in good agreement with the field characteristics of the pennant veins, since pennant terminations are in the extensional quadrant as predicted by the analogue modelling. WNW-ESE sinistral shear also justifies the down-to-the-south displacement shown by the striae observed in the interconnecting surfaces of the pennant veins (Fig. 5). On a regional scale, the WNW-ESE sinistral shear can be interpreted as associated with the E-W shortening responsible for the large scale folding. Both sets of veins are ascribable to the convergent stage of M2 (M2c) and therefore late with respect to the main wrench stage that produced the lineation. The fact that sigmoidal veins deflect the main lineation and that both sets develop under retrograde metamorphic conditions further support this conclusion. Crenulation cleavage and lineations parallel to early M2w lineations is present in the micaschist interbeds and the associated

folding is only visible on map scale, but the sigmoidal and pennant veins are the only mesoscopic evidence of M2c present in the quartzitic layering of the study area.

7. Conclusions

This paper introduces *pennant veins*, a new type of vein geometry with a geometry similar to established types such as sigmoidal tension gashes, wing cracks and wordtail and fishmouth termination veins. Analogue modelling has shown that pennant terminations are controlled by the kinematics of Riedel conjugate sets of fractures. The space available for vein deposition is obtained by combined rotation of and slip in the operating shear fractures. The orientation of pennant terminations is expected to be in the extensional quadrant of the bulk flow and, if combined with other criteria, can be used as a shear sense indicator. Care has to be taken to distinguish between *R*-dominated and *R′* dominated veins in such cases. However, neither the interconnecting nor the external surfaces of pennant veins correspond to the maximum shortening direction of the ISA as in tension gashes, but depend on the orientation of the *R*/*R′* conjugate set in a given moment of deformation. This observation, together with the uncertainty of the amount of rotation of shear fractures in natural examples, hinders the use of pennant veins as reliable gauges for bulk flow.

Acknowledgements

The experiments were preformed in LATTEX – Laboratório de Tectonofísica e Tectónica Experimental (Universidade de Lisboa). SC is grateful for the funding provided by Fundação para a Ciência e Tecnologia (SFRH/BD/12221/2003) and to Rüdiger Killian and Eric de Kemp for company during fieldwork. CWP and SC thank the Schürmann Foundation for logistical support and financial aid in Namibia. This work is also a contribution to TEAMINT (POCTI/CTA48137/2002). Reviews from Mark Swanson and Paul Williams are gratefully acknowledged.

References

Ahlgren, S.G., 2001. The nucleation and evolution of Riedel shear zones as deformation bands in porous sandstone. Journal of Structural Geology 23, 1203–1214.

Bartlett, W.L., Friedman, M., Logan, J.M., 1981. Experimental folding and faulting of rocks under confined pressure. Part IX. Wrench faults in limestone layers. Tectonophysics 79, 255–277.

Bons, P.D., 2000. The formation of veins and their microstructures. In: Jessel, M.W., Urai, J.L. (Eds.), Stress, strain and structure, a volume in honour of W.D. Means. Journal of the Virtual Explorer 2.

Bose, S., Marques, F.O., 2004. Controls on the geometry of tails around rigid circular inclusions: insights from analogue modelling in simple shear. Journal of Structural Geology 26, 2145–2156.

Braun, J., 1994. Three-dimensional numerical simulations of crustal scale wrenching using a non-linear failure criterion. Journal of Structural Geology 16, 1173–1186.

Cloos, E., 1955. Experimental analysis of fracture patterns. Geological Society of America Bulletin 66, 241–256.

Cooke, M.L., 1997. Fracture localization along faults with spatially varying friction. Journal of Geophysical Research 102, 22425–22434.

Cruikshank, K.M., Zhao, G., Johnson, A.M., 1991. Analysis of minor fractures associated with joints and faulted joints. Journal of Structural Geology 13, 865–886.

Davis, G.H., Bump, A.P., Garcia, P.E., Ahlgren, S.G., 1999. Conjugate Riedel deformation band shear zones. Journal of Structural Geology 22, 169–190.

Dresen, G., 1991. Stress distribution and the orientation of Riedel shears. Tectonophysics 188, 239–247.

Galland, O., de Bremond d'Ars, J., Cobbold, P.R., Hallot, E., 2003. Physical models of magmatic intrusion during thrusting. Terra Nova 15 (6), 405–409.

Goscombe, B., Hand, M., Gray, D., 2003a. Structure of the Kaoko Belt, Namibia: progressive evolution of a classic transpressional orogen. Journal of Structural Geology 25, 1049–1081.

Goscombe, B., Hand, M., Gray, D., Mawby, J., 2003b. The metamorphic architecture of a transpressional orogen: the Kaoko Belt, Namibia. Journal of Petrology 44, 679–711.

Goscombe, B., Gray, D., Hand, M., 2005a. Extrusional tectonics in the core of a transpressional orogen: the Kaoko Belt, Namibia. Journal of Petrology 46, 1203–1241.

Goscombe, B., Gray, D., Armstrong, R., Foster, D.A., Vogl, J., 2005b. Event geochronology of the Pan-African Kaoko Belt, Namibia. Precambrian Research 140, 103. e1-103-e.41.

Hanmer, S., 1986. Asymmetrical pull-aparts and foliation fish as kinematic indicators. Journal of Structural Geology 8, 111–115.

Hilgers, C., Urai, J.L., 2002. Microstructural observations on natural syntectonic fibrous veins: implications for the growth process. Tectonophysics 352, 257–274.

Hoffman, P.F., Swart, R., Freyer, E.E., Guowei, H., 1994. Damara Orogen of Northwest Namibia. In: Niall, M., McManus, C. (Eds.), Geological Excursion Guide of the International Conference Proterozoic Crustal and Metallogenetic Evolution. Geological Society and Geological Survey of Namibia, 55 pp.

Horii, H., Nemat-Nasser, S.J., 1985. Compression-induced microcracks growth in brittle solids: axial splitting and shear failure. Journal of Geophysical Research 90, 3105–3125.

Katz, Y., Weinberger, R., Aydin, A., 2004. Geometry and kinematic evolution of Riedel shear structures, Capitol Reef National Park, Utah. Journal of Structural Geology 26, 491–501.

Köhn, D., Hilgers, C., Bons, P.D., Passchier, C.W., 2000. Numerical simulations of fibre growth in antitaxial strain fringes. Journal of Structural Geology 22, 1311–1324.

Konopásek, J., Kröner, S., Kitt, S.L., Passchier, C.W., Kröner, A., 2005. Oblique collision and evolution of large-scale transcurrent shear zones in the Kaoko belt, NW Namibia. Precambrian Research 136, 139–157.

Krantz, R.W., 1991. Measurements of friction coefficients and cohesion for faulting and fault reactivation in laboratory models using sand and sand mixtures. In: Cobbold, P.R. (Ed.), Experimental and Numerical Modelling of Continental Deformation. Tectonophysics 188, 203–207.

Marques, F.O., 2001. Flow and fracturing of clay: analogue experiments in pure shear. Tectonic Modeling: A Volume in Honor of Hans Ramberg. Geological Society of America Bulletin, Memoir 193, 261–270.

Marques, F.O., Coelho, S., 2001. Rotation of rigid elliptical cylinders in viscous simple shear flow: analogue experiments. Journal of Structural Geology 23, 609–617.

Marques, F.O., Bose, S., 2004. Influence of a permanent low-friction boundary on rotation and flow in rigid inclusion/viscous-matrix systems from an analogue perspective. Tectonophysics 382, 229–245.

Martel, S.J., Pollard, D.D., 1989. Mechanics of slip and fracture along small faults and simple strike-slip fault zones in granitic rock. Journal of Geophysical Research 94, 9417–9428.

McKinnon, S.D., Garrido de la Barra, I., 1998. Fracture initiation, growth and effect on stress field: a numerical investigation. Journal of Structural Geology 20, 1673–1689.

Moore, D.E., Byerlee, J., 1992. Relationships between sliding behaviour and internal geometry of laboratory fault zones and some creeping and locked strike-slip faults of California. Tectonophysics 211, 305–316.

Moore, J.M., 1979. Tectonics of the Najd transcurrent fault system, Saudi Arabia. Journal of the Geological Society of London 136, 441–454.

Naylor, M.A., Mandl, G., Sijpesteijn, C.H.K., 1986. Fault geometries in basement-induced wrench faulting under different initial stress states. Journal of Structural Geology 8, 737–752.

Nemat-Nasser, S., Horii, H., 1982. Compression induced nonplanar crack extension with application to splitting, exfoliation and rockburst. Journal of Geophysical Research 87, 6805–6821.

Olson, J.E., Pollard, D.D., 1991. The initiation and growth of en echelon veins. Journal of Structural Geology 13, 595–608.

Passchier, C.W., Trouw, R.A.J., 2005. Microtectonics, second ed. Springer-Verlag.

Passchier, C.W., Trouw, R.A.J., A. Ribeiro, A., Paciullo, F.V.P., 2002. Tectonic evolution of the southern Kaoko belt, Namibia. Journal of African Earth Sciences 35, 61–75.

Ramsay, J.G., Huber, M.I., 1983. The Techniques of Modern Structural Geology. Volume 1: Strain Analysis. Academic Press, London.

Riedel, W., 1929. Zur Mechanik geologischer Brucherscheinungen. Zentralblatt für Mineralogie Abteilung B, 354–368.

Schreus, G., 1994. Experiments on strike-slip faulting and block rotation. Geology 22, 567–570.

Smith, J.V., Durney, D.W., 1992. Experimental formation of brittle structural assemblages in oblique divergence. Tectonophysics 216, 235–253.

Swanson, M.T., 1992. Late Acadian-Alleghian transpressional deformation: evidence from asymmetric boudinage in the Casco Bay area, coastal Maine. Journal of Structural Geology 14, 323–341.

Tchalenko, J.S., 1968. The evolution of kink bands and the development of compression textures in sheared clays. Tectonophysics 6, 159–174.

Weijermars, R., 1986. Flow behaviour and physical chemistry of bouncing putties and related polymers in view of tectonic laboratory applications. Tectonophysics 124, 325–358.

Wilcox, R.E., Harding, T.P., Seely, D.R., 1973. Basic wrench tectonics. The American Association of Petroleum Geologists Bulletin 57, 74–96.

Willemse, E.J.M., Pollard, D.D., 1998. On the orientation and patterns of wing cracks and solution surfaces at the tips of a sliding flaw or fault. Journal of Geophysical Research 103, 2417–2438.